Green's functions in full-potential multiple-scattering theory

A. Rusanu and G. M. Stocks
Materials Science and Technology Division, Oak Ridge National Laboratory, Oak Ridge, Tennessee 37831, USA

Y. Wang
Pittsburgh Supercomputing Center, Carnegie Mellon University, Pittsburgh, Pennsylvania 15213, USA

J. S. Faulkner
Department of Physics, Florida Atlantic University, Boca Raton, Florida 33486, USA

(Received 3 June 2011; published 13 July 2011)

One-electron Green's functions play a central role in multiple-scattering theory (MST) based electronic-structure methods. Robust methods exist for calculating the Green's function for crystal potentials that are spherically symmetric about atomic centers. When applied to potentials of general shape, these same techniques result in pathologies in the small-r behavior of the electronic charge density because a portion of the Green's function can become singular at the origin for that case. We propose an algebraic method that eliminates the singular behavior by making use of the equivalence of two terms that involve poles in the inverse of the sine matrix. Our accurate calculations illustrate the limitations of previous methods for treating this problem that rely on extrapolating the solutions near the origin.

DOI: 10.1103/PhysRevB.84.035102 PACS number(s): 71.15.Ap, 71.15.Dx

I. INTRODUCTION

The multiple-scattering theory (MST) of Rayleigh,[1] Korringa,[2] Kohn, and Rostoker[3] has found its most widespread application in the calculation of one-electron Green's functions for solids and other large aggregates of atoms. MST calculations are much easier if the one-electron potential functions from the density-functional theory (DFT)[4] are forced into the muffin-tin form. A muffin-tin (MT) potential is spherically symmetric within nonoverlapping muffin-tin spheres that enclose the nuclei of each atom, and constant between these spheres. It is a good approximation for crystalline metals, but it introduces unacceptable errors in many applications. When standard MST is used in full-potential calculations, the r dependence of the coefficients $\rho_\ell(r)$ in a spherical expansion of the calculated charge density can be pathological for values of r that are a sizeable fraction of the muffin-tin radius. The pathologies become worse as ℓ increases. Techniques for eliminating these pathologies have been suggested,[5] and there have been books written on the subject.[6] We investigated these techniques and found them unsatisfactory for our purposes. In this paper, we describe a new approach to the problem that removes the pathological behavior and gives $\rho_\ell(r)$ that are well-converged for all r. It is based on a subtle mathematical equivalence that was posited by one of the authors.[7] A preliminary report has been presented.[8]

In principle, the elimination of the muffin-tin approximation is straightforward. It is generally agreed that the form of the MST Green's function that was derived some time ago[9] is applicable to potentials that have no shape approximation. When $\mathbf{r}$ and $\mathbf{r}'$ are in the nth cell and $r' > r$, it is written

$$G(E,\mathbf{r},\mathbf{r}') = \sum_L \sum_{L'} Z_L^n(E,\mathbf{r})\tau_{LL'}^{nn}(E)Z_{L'}^{n\bullet}(E,\mathbf{r}') - \sum_L Z_L^n(E,\mathbf{r})J_L^{n\bullet}(E,\mathbf{r}'), \quad (1)$$

where L stands for the pair of angular-momentum indices ℓ and m. The $Z_L^n(E,\mathbf{r})$ are obtained by integrating outward from the origin at the nucleus of atom n, and are regular there. The $J_L^n(E,\mathbf{r})$ satisfy a boundary condition away from the nucleus and are obtained by integrating inward. There is no reason for them to be regular at the origin, and they typically approach infinity there.[10] The scattering-path matrices $\tau_{LL'}^{nn}(E)$ describe the propagation of the electron around all paths in the solid, and will be described below in more detail.

Parameters that are used to describe the electronic structure of condensed matter can be obtained from the Green's function. The ones that are needed for calculating the self-consistent total energy are the density of states,

$$n(E) = -\frac{2}{\pi V}\mathrm{Im}\int_V G(E,\mathbf{r},\mathbf{r})d\mathbf{r}, \quad (2)$$

the charge density,

$$\rho(\mathbf{r}) = -\frac{2}{\pi}\mathrm{Im}\int_{E_B}^{E_F} G(E,\mathbf{r},\mathbf{r})dE, \quad (3)$$

and the sum of one-electron eigenvalues,

$$\Sigma = \int_{E_B}^{E_F} En(E)dE. \quad (4)$$

In these equations, E_B is the lowest eigenvalue in the conduction band and E_F is the Fermi energy.

The straightforward application of Eq. (1) in the calculation of these parameters requires an amount of computational time that is almost prohibitive because $G(E,\mathbf{r},\mathbf{r}')$ varies rapidly with energy. The resolution of this problem follows from the observation that, when viewed as functions of complex energy $G(z,\mathbf{r},\mathbf{r}')$, Green's functions are holomorphic everywhere except for poles at the bound states and a cut on the part of the real axis starting at E_B and extending to plus infinity. Because $G(z,\mathbf{r},\mathbf{r}')$ is a much smoother function of z than of E, parameters that require an integral over energy are evaluated

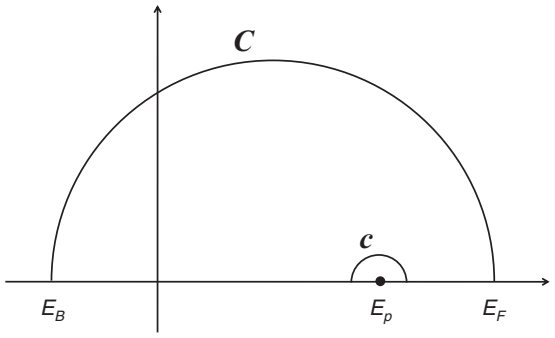

FIG. 1. In applications, various portions of the Green's function must be integrated from the bottom of the conduction band E_B, to the Fermi energy E_F. This integration can be carried out along the real axis or over the contour C in the complex-energy plane that connects E_B to E_F. Integrals over the small contour c, which encloses the pole of the inverse of the sine matrix E_p, are also useful.

by integrating over a contour in the upper half-plane that is restricted only by the conditions that it starts at E_B and ends at E_F.[11] This contour is labeled C in Fig. 1.

The singular second term in Eq. (1), which we call the *ZJ* term, is ignored when real energies are used because it is real and only the imaginary part of the Green's function appears in Eqs. (2)–(4). It is relatively easy to evaluate this term precisely for complex energies when the potentials have the MT form. The *ZJ* term can neither be ignored nor precisely evaluated for complex energies and full potentials. A method for dealing with this problem that is used extensively is to stop calculating *ZJ* within a sphere surrounding the origin and to extrapolate by some means within that sphere.[5,6] As will be shown, the correct charge density for the conduction electrons has undulations that reflect the orthogonality of the wave functions to the core functions and are appreciable at radii as small as the radius of the 1*s* electrons. Misrepresenting these undulations can lead to significant uncontrolled errors in the charge density, total energy, Hellmann-Feynman forces, and other physical quantities.

Using our new techniques, we have carried out full-potential MST calculations of the charge densities of the conduction electrons in copper and molybdenum. Some of the results are used to obtain the data in Table I, which validate our theoretical analysis. The components of the copper charge density, $\rho_\ell(r)$, are shown in Fig. 2, and the undulations described above are evident. Figures 4 and 5 show that the limiting behavior of the $\rho_\ell(r)$ is correct for very small r. We find that full-potential calculations are much easier for molybdenum than for copper.

TABLE I. Contributions to the total charge in the conduction band for copper and molybdenum. The unit of charge is e, i.e., the charge of an electron.

species	A_1	A_2	A_3	B_1	B_2
Cu (MT)	19.97178	−8.97178	19.60186	10.63008	8.97178
Cu (FP)	19.59501	na	19.22930	10.63428	8.59501
Mo (MT)	6.00000	0.0000	6.36651	6.36651	0.00000
Mo (FP)	6.00000	na	6.38959	6.38959	0.00000

This fact, which is by no means obvious from the atomic numbers of the elements, will be explained.

II. THEORY

There are reasons that one-electron Green's functions play such a central role in multiple-scattering theory (MST) based electronic structure methods. As illustrated above, most parameters of interest can easily be calculated from them. They can be averaged over different configurations to yield the coherent potential approximation (CPA) for substitutional alloys.[12] Equations that describe localized impurities in solids are obtained from them.[13] The order-N locally self-consistent multiple-scattering (LSMS) method,[14] which can be used to find the electronic structure for large numbers and arbitrary configuration of atoms, is based on them.

From the eigenvalue expansion of the Green's function it can be seen to have poles at the discrete eigenvalues E_i that correspond to the bound states of the atoms. The eigenvalues in the conduction band fall in a branch cut that extends from the bottom of the band E_B to plus infinity. The function $G(z,\mathbf{r},\mathbf{r}')$ is therefore holomorphic on the cut plane, the cut extending on the real energy axis from the lowest bound-state eigenvalue E_0 to infinity. The value of the Green's function is defined on the real axis as $G(E,\mathbf{r},\mathbf{r}') = \lim_{z\downarrow E} G(z,\mathbf{r},\mathbf{r}')$.

The scattering-path operators $\tau^{nn}_{LL'}(E)$ introduced in Eq. (1) are defined as follows. Divide space into a collection of nonoverlapping polyhedra Ω_n, the center of each polyhedron, $\mathbf{R}_n$, being the location of the nucleus of one of the atoms in the solid. The one-electron potential is written $V(\mathbf{r}) = v_n(\mathbf{r})$, when $\mathbf{r} \subset \Omega_n$.When $\mathbf{r}$ and $\mathbf{r}'$ are both in Ω_n and $|\mathbf{r}'| > |\mathbf{r}|$, the Green's function is written as in Eq. (1) with

$$\tau^{nn}_{LL'}(E) = t^n_{LL'}(E) + \sum_{k\neq n=1}^{N} \sum_{L_1} \sum_{L_2} t^n_{LL_1}(E)\, g^{nk}_{L_1L_2}(E)\, \tau^{kn}_{L_2L'}(E), \quad (5)$$

where the $t^n_{LL'}(E)$ are the elements of the t matrix that describes the scattering from the potential $v_n(\mathbf{r})$. The $g^{nk}_{L_1L_2}(E)$ are free-electron Green's functions that propagate the electron from site n to site k.

It is useful to define the t matrix in terms of sine and cosine matrices

$$\mathbf{t}^n = -\frac{1}{\alpha}\mathbf{s}^n(\mathbf{c}^n - i\mathbf{s}^n)^{-1}. \quad (6)$$

It has been shown[15] that these matrices can best be calculated with the help of an ancillary function $\varphi^n_L(E,\mathbf{r})$ that is the solution of

$$[-\nabla^2 + v_n(\mathbf{r})]\varphi^n_L(E,\mathbf{r}) = E\varphi^n_L(E,\mathbf{r}), \quad (7)$$

and satisfies the boundary condition

$$\lim_{r\to 0} \varphi^n_L(E,\mathbf{r}) = Y_L(\mathbf{r})\, j_l(\alpha r). \quad (8)$$

In this equation, $j_l(\alpha r)$ is the spherical Bessel function that is regular at the origin, $\alpha = \sqrt{E}$, and $Y_L(\mathbf{r})$ is the spherical harmonic with the angles (ϑ,φ) defined by the direction of the vector $\mathbf{r}$. It is obvious that for $r > R^n_c$, where R^n_c is the radius of the sphere that circumscribes Ω_n, $\varphi^n_L(E,\mathbf{r})$ can be written

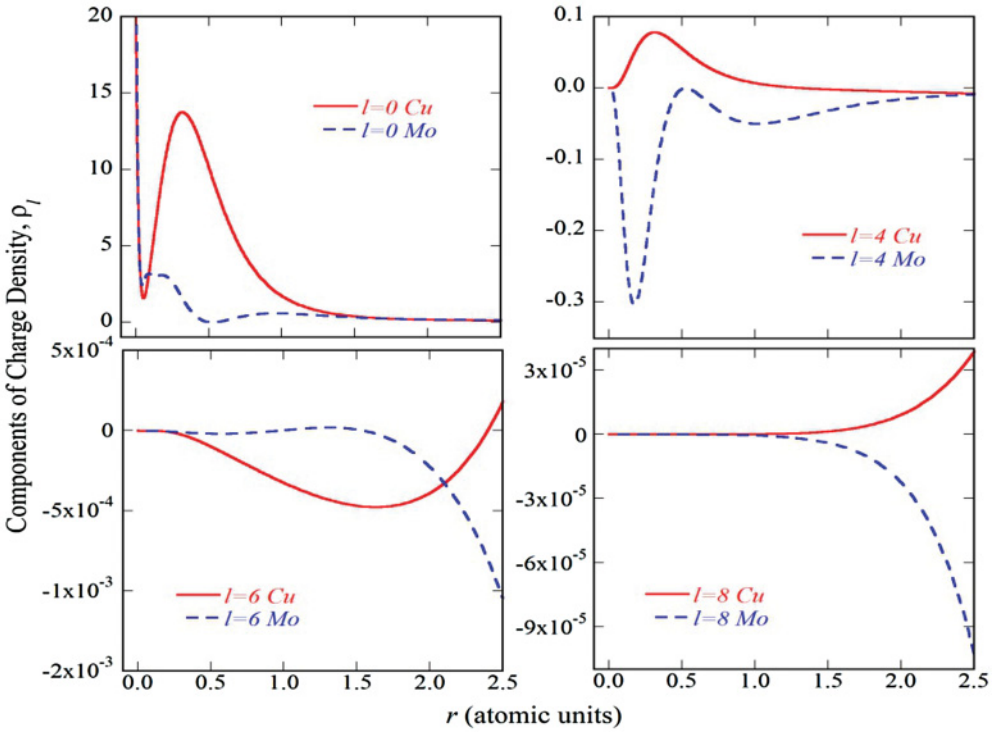

FIG. 2. (Color online) The components of the valence-band charge density (ρ_l) of Cu and Mo corresponding to $\ell = 0,4,6$, and 8. The charge is in electron charges and r is in Bohr radii.

as a linear combination of the $j_l(\alpha r)$ and the spherical Bessel functions of the second kind, $n_l(\alpha r)$,

$$\varphi_L^n(E,\mathbf{r}) = \sum_{L'} Y_{L'}(\mathbf{r})\left[n_{l'}(\alpha r)\, s_{L'L}^n(E) - j_{l'}(\alpha r)\, c_{L'L}^n(E)\right]. \tag{9}$$

By comparing this function with a solution of Eq. (7) in the scattered wave form, it can be shown that the coefficients are the elements of the sine and cosine matrices. It is by no means obvious, but it has been shown by exhaustive computational and algebraic studies,[16] that Eq. (9) holds true for $r < R_c^n$ as long as $\mathbf{r}$ is on the surface or outside of the polyhedron Ω_n.

Formulas for the sine and cosine matrices can be found by using the Wronskian relations satisfied by the Bessel functions. They are

$$S_{L_1L_0}^n = \alpha \iint_{S_n} \{j_{l_1}(\alpha r)Y_{L_1}^*(\mathbf{r}), \varphi_{L_0}^n(E,\mathbf{r})\} \cdot \mathbf{n} dS, \tag{10}$$

and

$$C_{L_1L_0}^n = \alpha \iint_{S_n} \{n_{l_1}(\alpha r)Y_{L_1}^*(\mathbf{r}), \varphi_{L_0}^n(E,\mathbf{r})\} \cdot \mathbf{n} dS, \tag{11}$$

where S_n is the surface of the polyhedron Ω_n. The curly brackets indicate a three-dimensional Wronskian, $\{f,g\} = f\nabla g - g\nabla f$. Using Gauss's theorem, these equations can be rewritten as volume integrals

$$S_{L_1L_0}^n = \alpha \iiint_{\mathbf{r}\subset\Omega_n} j_{l_1}(\alpha r)Y_{L_1}^*(\mathbf{r})v_n(\mathbf{r})\varphi_{L_0}^n(E,\mathbf{r})d\mathbf{r}' \tag{12}$$

and

$$C_{L_1L_0}^n = \alpha \iiint_{\mathbf{r}\subset\Omega_n} n_{l_1}(\alpha r)Y_{L_1}^*(\mathbf{r})v_n(\mathbf{r})\varphi_{L_0}^n(E,\mathbf{r})d\mathbf{r}' - \delta_{L_1L_0} \tag{13}$$

The functions $Z_L^n(E,\mathbf{r})$ that appear in Eq. (1) are linear combinations of the $\varphi_L^n(E,\mathbf{r})$:

$$Z_L^n(E,\mathbf{r}) = \alpha \sum_{L'} \varphi_{L'}^n(E,\mathbf{r})\, s_{L'L}^{n-1}(E), \tag{14}$$

so they are also regular at the origin. The $J_L^n(E,\mathbf{r})$, however, are solutions of

$$[-\nabla^2 + v_n(\mathbf{r})]J_L^n(E,\mathbf{r}) = E J_L^n(E,\mathbf{r}) \tag{15}$$

that take on the asymptotic values

$$J_L^n(E,\mathbf{r}) \to Y_L(\mathbf{r})\, j_l(\alpha r) \tag{16}$$

when $\mathbf{r}$ is outside the range of the potential $v_n(\mathbf{r})$, $r > R_c^n$. These functions are typically infinite at $\mathbf{r} = 0$.

As a last point about the notation of Eq. (1), it will be noticed that we use a dot on certain functions $F^\bullet$ when one might expect the asterisk that would indicate complex conjugation F^*. The dot indicates that we take the complex conjugate of any spherical harmonics that are involved, but we leave the remainder of the function unchanged. The necessity for such an operation arises from the fact that it produces a conjugate Green's function that yields the symmetry

$$G(E,\mathbf{r},\mathbf{r}')^\bullet = G(E,\mathbf{r}',\mathbf{r}). \tag{17}$$

As an example, the dot of the cosine matrix gives

$$c^{n\bullet}_{l_1,m_1,l_2,m_2} = (-1)^{m_1+m_2}\, c^{n}_{l_1,-m_1,l_2,-m_2}. \tag{18}$$

One of the authors, Y. Wang, derived a useful lemma starting from the observation that

$$\nabla \cdot \left\{\varphi^{n\bullet}_{L'}(E,\mathbf{r}),\varphi^{n}_{L}(E,\mathbf{r})\right\} = 0. \tag{19}$$

Integrating this divergence over Ω_n and using Gauss's theorem again, it follows that

$$\iint_{S_n} \left\{\varphi^{n\bullet}_{L'}(E,\boldsymbol{r}),\varphi^{n}_{L}(E,n\boldsymbol{r})\right\}.\boldsymbol{n}dS = 0. \tag{20}$$

From this equation and Eqs. (9)–(11), it can be shown that the sine and cosine matrices satisfy

$$\tilde{\mathbf{c}}^{n\bullet}\mathbf{s}^{n} - \tilde{\mathbf{s}}^{n\bullet}\mathbf{c}^{n} = 0, \tag{21}$$

where the tilde indicates the transpose of the matrix. Wang's lemma can be used to prove

$$\tilde{\mathbf{t}}^{n\bullet} = \mathbf{t}^{n}, \tag{22}$$

and

$$\tilde{\tau}^{nn\bullet} = \tau^{nn}, \tag{23}$$

which are necessary for demonstrating the symmetry relation in Eq. (17).

The above equations are simplified when the potential has the MT form because all of the sine, cosine, and t matrices are diagonal. It was thought at one time that the MST would have to be fundamentally changed to treat full potentials, but that is no longer the prevailing view. The only approximation that must be made in practical calculations is that the dimensions of the scattering matrices are kept finite by ignoring contributions from angular momenta greater than some $\ell_{\max}$.

As pointed out in the introduction, calculations with MST Green's functions can be sped up dramatically by carrying out the energy integrations in formulas such as Eqs. (3) and (4) along the contour C in the complex plane as sketched in Fig. 1 rather than along the real axis. The price that must be paid is that it introduces problems with the ZJ term. The problems with the ZJ term have been dealt within one way or another by all the groups that do full-potential MST calculations.

The two terms in Eq. (1) will be abbreviated $Z\tau Z$ and ZJ. They are holomorphic individually, so we can choose different contours of integration for them. In particular, we can integrate the $Z\tau Z$ term along the complex contour and the ZJ term along the real axis. By the argument given above, the ZJ term would make no contribution, and the problem would be solved. That works for some materials but not for others, so a more detailed analysis is necessary.

The ZJ term has nothing to do with multiple scattering. It appears in the Green's function that describes propagation in the potential $v_n(\mathbf{r})$ alone

$$G_n(E,\mathbf{r},\mathbf{r}') = \sum_{L}\sum_{L'} Z^{n}_{L}(E,\mathbf{r})t^{n}_{LL'}Z^{n\bullet}_{L'}(E,\mathbf{r}') - \sum_{L} Z^{n}_{L}(E,\mathbf{r})J^{n\bullet}_{L}(E,\mathbf{r}'). \tag{24}$$

Using Eq. (6) and Wang's lemma, Eq. (21), the t matrix for the single scatterer can be written

$$\mathbf{t}^{n} = -\frac{1}{\alpha}\mathbf{s}^{n}\,\Xi^{-1}[\tilde{\mathbf{c}}^{n\bullet} - i\tilde{\mathbf{s}}^{n\bullet}], \tag{25}$$

where

$$\Xi = \tilde{\mathbf{c}}^{n\bullet}\mathbf{c}^{n} + \tilde{\mathbf{s}}^{n\bullet}\mathbf{s}^{n}. \tag{26}$$

Using Eq. (14), the Green's function becomes

$$G_n(E,\mathbf{r},\mathbf{r}') = i\alpha\sum_{L}\sum_{L}\phi^{n}_{L}(E,\mathbf{r})\Xi^{-1}_{LL'}\phi^{n\bullet}_{L'}(E,\mathbf{r}') - \alpha\sum_{L}\sum_{L'}\sum_{L_1}\sum_{L_2}\phi^{n}_{L}(E,\mathbf{r})\Xi^{-1}_{LL_1}\tilde{c}^{n\bullet}_{L_1L_2}\tilde{s}^{n\bullet-1}_{L_2L'}\phi^{n\bullet}_{L'}(E,\mathbf{r}') - \alpha\sum_{L}\sum_{L'}\phi^{n}_{L}(E,\mathbf{r})s^{n-1}_{LL'}J^{n\bullet}_{L'}(E,\mathbf{r}). \tag{27}$$

For real energies, the first term in Eq. (27), which we call $(ZtZ)_1$, is pure imaginary. The poles of the inverse matrices that appear in Eq. (27) are identified by recalling that a matrix inverse is the matrix of cofactors divided by the determinant. The function $\det\Xi$ is only zero when the energy corresponds to a bound state for the potential $v_n(\mathbf{r})$. Bound states are not affected by the other atoms, and hence are easy to treat. Their eigenvalues fall in the range $E_0 < E < E_B$. In MST, we are only interested in energies in the conduction band that fall in the interval (E_B,E_F), so Ξ^{-1} can be considered as a matrix with no poles. The second and third terms, which we call $(ZtZ)_2$ and ZJ are real on the real axis. They have poles at the energies E_p for which $\det\mathbf{s}^{n} = 0$, and that means they can contribute to the imaginary part of the Green's function if a pole energy E_p falls within (E_B,E_F).

The contributions to the imaginary part of the Green's function from the pole in ZJ and $(ZtZ)_2$, which we call $(ZJ)^p$ and $(ZtZ)^p_2$, must cancel:

$$(ZtZ)^{p}_{2} - (ZJ)^{p} = 0, \tag{28}$$

because the Green's functions $G(z,\mathbf{r},\mathbf{r}')$ or $G_n(z,\mathbf{r},\mathbf{r}')$ have no poles at E_p. It follows that the energy integrals of the imaginary part of the Green's function can be carried out by integrating the contribution

$$F_1(E,\mathbf{r},\mathbf{r}') = \sum_{L}\sum_{L'} Z^{n}_{L}(E,\mathbf{r})\left(\tau^{nn}_{LL'} - t^{n}_{LL'}\right)Z^{n\bullet}_{L'}(E,\mathbf{r}'), \tag{29}$$

over the complex contour C and the $(ZtZ)_1$ term,

$$F_2(E,\mathbf{r},\mathbf{r}') = i\alpha\sum_{L}\sum_{L}\phi^{n}_{L}(E,\mathbf{r})\Xi^{-1}_{LL'}\phi^{n\bullet}_{L'}(E,\mathbf{r}'), \tag{30}$$

along the real axis. This is a mathematically correct way to eliminate the $J_L^n(E,\mathbf{r})$ from the imaginary part of the Green's function and it can give the same accurate charge densities as shown in Fig. 2. However, as is explained below, this is not a practical way to perform full-potential calculations because of its laboriousness for systems that present sharp d or f resonances. A much better way is described in connection with Eq. (32). The algebra that leads to Eqs. (29) and (30) is similar to an argument that was put forward previously,[17,18] but, so far as we know, it was never used in the way that we have described.

The imaginary part of the contribution in Eq. (29) is a rough function of the energy because it contains the density of states for the entire solid, but it is integrated over the contour C where it is smooth. The contribution from the $(ZtZ)_1$ term is proportional to the density of states for the single site. From Friedel's rule, this looks like the derivative of the phase shifts. For systems containing transition metals, which have resonances in the d channel, there are sharp peaks at the resonances. For systems containing rare earths or actinides, which have resonances in the f channel, the peaks are even sharper. This is illustrated in Fig. 3 in which we show the density of states,

$$n_n(E) = -\frac{2\alpha}{\pi}\sum_L\sum_{L'}\int_{\Omega_n}\phi_L^n(E,\mathbf{r})\,\Xi^{-1}_{LL'}\phi_{L'}^{n\bullet}(E,\mathbf{r})\,d\mathbf{r} \quad (31)$$

for full-potential copper. This curve is certainly smooth compared with the density of states of the solid, but still a large number of energy points are required to calculate the contribution from the region near such a resonance. This is not a problem for MT or ASA calculations, where the calculation of the t matrices take little time compared with the calculation of the τ matrix, but it is a bottleneck in full-potential calculations, where the time to calculate the sine and cosine matrices is significant and the minimization of the number of evaluations of these matrices is crucial.

There is a better way to eliminate the inward integrations using a method that is described most readily with the help of the sketch of energy contours in Fig. 1. Going back to Eq. (1),

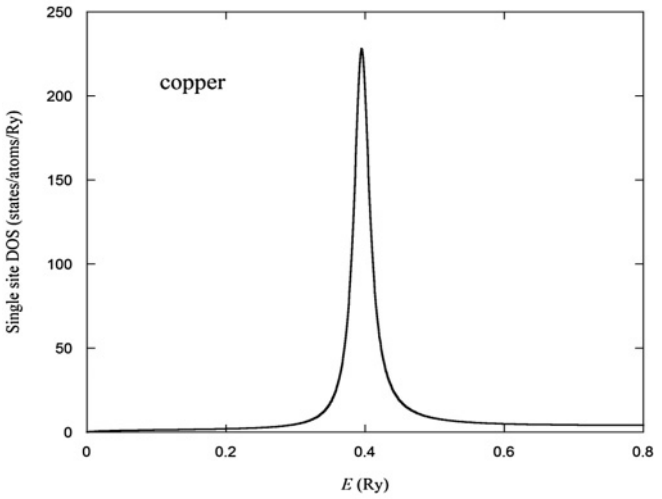

FIG. 3. The single-site density of states for full-potential Cu, $n_n(E)$. The peak arises from a resonance in the d channel.

we integrate the first term $Z\tau Z$ along the complex contour C. The second term ZJ is integrated along the real axis from E_B to E_F so the only part of it that contributes to the imaginary part of the Green's function is, if $E_B < E_p < E_F$, the term $(ZJ)^p$ due to the pole at E_p. At first sight, this reintroduces the problem of the singularity at the origin, but it has been observed[7] that the equivalence in Eq. (28) implies that

$$(ZJ)^p = -\mathrm{Im}\int_c\sqrt{z}\sum_L\sum_{L'}\sum_{L_1}\sum_{L_2}\phi_L^n(z,\mathbf{r})\,\Xi^{-1}_{LL_1}\times\tilde{c}^{n\bullet}_{L_1L_2}\tilde{s}^{n\bullet-1}_{L_2L'}\phi_{L'}^{n\bullet}(z,\mathbf{r}')dz, \quad (32)$$

which does not contain the irregular function $J_L^n(E,\mathbf{r})$. Of course, if E_p does not fall in the interval of interest (E_B,E_F), $(ZJ)^p = 0$ and the integration of $Z\tau Z$ along the contour C is equivalent to integrating the entire Green's function. In either case, there is no need to integrate ZJ on the contour C. The resolution of the conundrum posed in the introduction is that E_p falls in (E_B,E_F) for copper but it does not for molybdenum, as will be demonstrated below.

The first thought is that the integral in Eq. (32) is just π times the residue at E_p, so a closed expression could be obtained for $(ZJ)^p$. Calculating the residue analytically works well for certain simple cases, but very often the order of the pole is greater than one. The number of points on contour c that are required for acceptable accuracy is quite small (4–8 points), so it is usually better to do the integral than to find the residue algebraically. Computationally, the locations of E_p can be readily determined by a binary search algorithm of the zeros of the $\det\mathbf{s}^n$ and a contour of radius 10^{-5}–10^{-4} is found to yield accurate results.

III. CALCULATIONS

In Table I, we show the results of calculations of certain contributions to the total charge in the conduction band for copper and molybdenum that were carried out with codes based on the real-space locally self-consistent multiple-scattering (LSMS) method. It would have been equally appropriate to use a more conventional KKR band-theory method, but, for the present purposes, there would be no functional difference in the results. The only significant approximation is the truncation of angula-momentum expansions. The scattering matrices are truncated at $\ell_{\max} = 4$, which means that the potentials and charge densities are expanded to $\ell_{\max} = 8$. These contributions are a compact way of demonstrating the relations derived in the preceding section.

The entries A_1 and A_2 for copper in Table I are obtained by integrating the imaginary parts of the terms in Eq. (1) over the complex-energy contour C shown in Fig. 1 and the atomic cell Ω,

$$A_1 = \mathrm{Im}\int_{\Omega_n}\int_C\sum_L\sum_{L'}Z_L^n(z,\mathbf{r})\tau^{nn}_{LL'}Z_{L'}^{n\bullet}(z,\mathbf{r})dzd\mathbf{r}, \quad (33)$$

$$A_2 = -\mathrm{Im}\int_{\Omega_n}\int_C\sum_L Z_L^n(z,\mathbf{r})\,J_L^{n\bullet}(z,\mathbf{r})dzd\mathbf{r}. \quad (34)$$

The integral over C of the first term in Eq. (24) gives the contribution A_3,

$$A_3 = \mathrm{Im} \int_{\Omega_n} \int_C \sum_L \sum_{L'} Z_L^n(z,\mathbf{r}) t_{LL'}^n Z_{L'}^{n\bullet}(z,\mathbf{r}) dz d\mathbf{r}. \quad (35)$$

For the purpose of illustration, the calculations in the first and third rows were done using MT potentials because otherwise we do not get values for the ZJ term A_2. The integral over the real axis of the first term in Eq. (27) is

$$B_1 = \mathrm{Im} \int_{\Omega_n} \int_{E_B}^{E_A} \sqrt{E} \sum_L \sum_{L'} \phi_L^n(E,\mathbf{r}) \Xi_{LL'}^{-1} \phi_{L'}^{n\bullet}\left(E,\mathbf{r}'\right) dE d\mathbf{r} = \mathrm{Im} \int_{\Omega_n} \int_{E_B}^{E_A} (ZtZ)_1 \, dE d\mathbf{r} \quad (36)$$

and the integral around the pole E_p of the second term gives

$$B_2 = \mathrm{Im} \int_{\Omega_n} \int_c \sqrt{z} \sum_L \sum_{L'} \sum_{L_1} \sum_{L_2} \phi_L^n(z,\mathbf{r}) \, \Xi_{LL_1}^{-1} \tilde{c}_{L_1L_2}^{n\bullet} \tilde{s}_{L_2L'}^{n\bullet -1} \phi_{L'}^{n\bullet}(z,\mathbf{r}) dz d\mathbf{r} = \mathrm{Im} \int_{\Omega_n} \int_c (ZtZ)_2 dz d\mathbf{r}. \quad (37)$$

The sum of A_1 and A_2 for MT copper is eleven, which is the number of the electrons in the conduction band. The sum of A_3 and A_2 is equal to B_1 because they are just two ways of calculating the one-atom contribution to the charge in the conduction band. Finally, from the discussion in the text, the term B_2 is equal to minus A_2 because their contributions from the poles at E_p are required to cancel each other. This is a numerical demonstration that our algebra is correct and we can replace A_2 with $-B_2$, which doesn't contain the irregular function $J_L^n(E,\mathbf{r})$. Full-potential numerical evaluations using $J_L^n(E,\mathbf{r})$ break the analyticity and the symmetry of the charge at small r, hence the integral over the large contour C of the ZJ term is not carried out in full-potential calculations, so we mark it "na". The correct number of electrons in the conduction band is obtained by replacing that contribution with $-B_2$.

The case of molybdenum shown in the third row of Table I is much simpler because there is no pole in the inverse of the sine matrix between E_B and E_F. Therefore, the term A_1 must be equal to the total number of electrons in the conduction band, which is six. Likewise, the term A_3 gives the entire one-atom contribution to the charge, which is the reason that it equals B_2. The full-potential calculations in the fourth row lead to results that are not greatly different from those obtained with the MT approximation.

The term that we call B_2 depends on the size of the contour that encloses the pole of the inverse of the sine matrix at E_p, whereas the ZJ term A_2 does not. As a practical matter, this means that we can only replace A_2 with $-B_2$ in the limit that the contour c has a zero radius. It is also the case that the term B_1 only gives the one-atom contribution to the charge when the integration is along the real axis. The reason for this is that the first term in Eq. (24) is holomorphic with a cut, but, when it is divided up as shown in Eq. (27), the fragments $(ZtZ)_1$ and $(ZtZ)_2$ are not holomorphic.

The data in Table I provide compelling evidence that the method that we propose for full-potential calculations based on Eq. (32) gives excellent results. However, there is much more information in the radial dependence of the charge densities that were integrated over to get those data. The charge density may be expressed as an expansion in spherical harmonics, $Y_{\ell,m}(\theta,\phi)$,

$$\rho(\mathbf{r}) = \sum_{\ell=0}^{8} \sum_{m=-\ell}^{\ell} \rho_{\ell,m}(r) Y_{\ell,m}(\theta,\phi). \quad (38)$$

As pointed out above, the scattering matrices in our calculations are truncated at $\ell_{\max} = 4$, so the charge densities are expanded to $\ell_{\max} = 8$.

From the group theory, we know that not all of the components $\rho_{l,m}(r)$ are independent. Metallic copper has the face-centered cubic crystal structure and metallic molybdenum has the body-center cubic crystal structure, so the charge density is invariant under the 48 operations of the full octahedral group. It follows that it can be expanded in terms of the basis functions for the trivial representation of that group,

$$\rho(\mathbf{r}) = \sum_{\ell=0}^{8} \rho_\ell(r) T_\ell(\theta,\phi). \quad (39)$$

The basis functions are written[19] in terms of the normalized real spherical harmonics

$$Y_{\ell,m}^c(\theta,\phi) = 2^{-1/2}[Y_{\ell,m}(\theta,\phi) + Y_{\ell,-m}(\theta,\phi)], \quad (40)$$

as

$$\begin{aligned}
T_0(\theta,\phi) &= Y_{0,0}(\theta,\phi), \\
T_4(\theta,\phi) &= \tfrac{1}{2}\sqrt{\tfrac{7}{3}} Y_{4,0}^c(\theta,\phi) + \tfrac{1}{2}\sqrt{\tfrac{5}{3}} Y_{4,4}^c(\theta,\phi), \\
T_6(\theta,\phi) &= \tfrac{1}{2}\sqrt{\tfrac{1}{2}} Y_{6,0}^c(\theta,\phi) - \tfrac{1}{2}\sqrt{\tfrac{7}{2}} Y_{6,4}^c(\theta,\phi), \\
T_8(\theta,\phi) &= \tfrac{1}{8}\sqrt{33} Y_{8,0}^c(\theta,\phi) + \tfrac{1}{4}\sqrt{\tfrac{7}{3}} Y_{8,4}^c(\theta,\phi) \\
&\quad + \tfrac{1}{8}\sqrt{\tfrac{65}{3}} Y_{8,8}^c(\theta,\phi).
\end{aligned}$$

The four independent components of the charge density $\rho_l(r)$ that appear in Eq. (39) are plotted for copper and molybdenum in Fig. 2. It is clear that the pathological behavior that is observed in these components when standard MST methods are used has been completely eliminated. In addition,

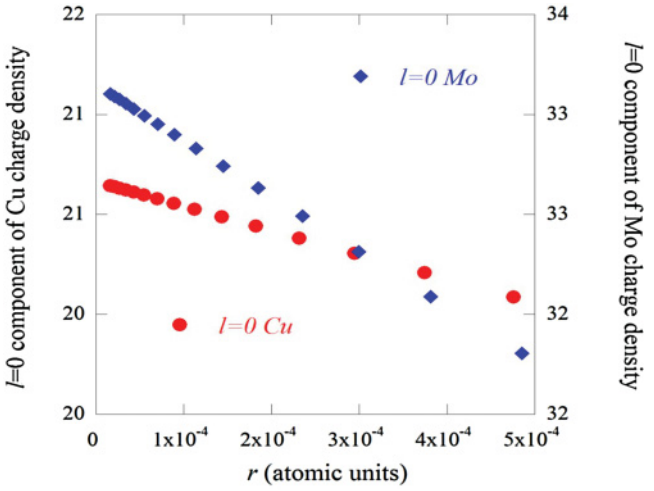

FIG. 4. (Color online) The component of the valence-band charge density of Cu and Mo corresponding to $\ell = 0$ for small r. The dots are at every 20th data point.

the undulations in the $\rho_\ell(r)$ required by the orthogonality of the band functions to the core states are clear, at least for $\ell = 0,4$, and 6. This is the most important result of the present study. It is hard to see how functions that are extrapolated for values of r within some fraction of the muffin-tin radius, which is 2.39 atomic units for Cu and 2.56 atomic units for Mo, can reproduce these undulations correctly.

Another test of the accuracy of our full-potential calculation is related to the behavior of the components $\rho_\ell(r)$ near the origin. For very small r, they take the form

$$\rho_\ell(r) \simeq A_\ell r^\ell e^{-\alpha_\ell r} \approx A_\ell r^\ell (1 - \alpha_\ell r). \tag{41}$$

From Fig. 4 it can be seen that $\rho_0(r)$ for Cu approaches a straight line with α_0 taking the value 57.35. This is very close to expected value of $\alpha_0 = 2Z = 58$. The data for Mo from the same figure also falls on a straight line with $\alpha_0 = 82.62$, which can be compared with the $2Z$ of 84. From Fig. 5 it can be seen that ρ_4/r^4 is a straight line for both Cu and Mo, with $\alpha_4 = 19.24$ for Cu. The slope of the line is in the opposite direction for Mo, with $\alpha_4 = -27.83$. This cusp behavior could not be obtained with a method that extrapolates $\rho_\ell(r)$ within any finite radius.

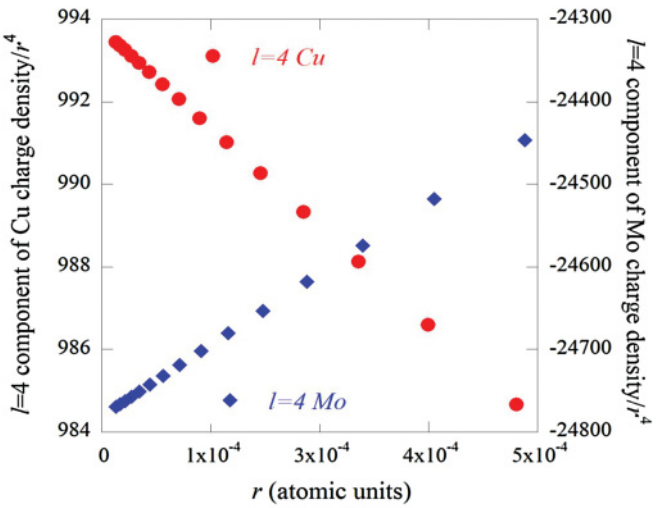

FIG. 5. (Color online) The component of the valence-band charge density of Cu and Mo corresponding to $\ell = 4$ divided by r^4. The dots are at every 20th data point.

IV. CONCLUSIONS

From Eq. (27), the source of the difficulty caused by the ZJ term in full-potential calculations can be seen. If the potential is spherical, the inverse of the sine matrix is diagonal and the only products that arise are of the form $\phi_L^n(E,\mathbf{r})J_L^{n\bullet}(E,\mathbf{r})$. A function that approaches infinity like $r^{-\ell-1}$ for small r is always multiplied by one that approaches zero like r^ℓ. In the full-potential case, we have terms like $\phi_L^n(E,\mathbf{r})s_{LL'}^{n-1}J_{L'}^{n\bullet}(E,\mathbf{r})$. If $L' \neq L$, the only way to prevent the product from being infinite near the origin is to calculate the functions and the matrix elements $s_{LL'}^{n-1}$ with unfeasible accuracy.

From the preceding sections, we conclude that the ZJ term should never be integrated over the large contour C. If the pole at E_p does not fall in (E_B, E_F), the integral of the $Z\tau Z$ term over the contour C is the integral of Green's function, as illustrated by the molybdenum calculations shown in Table I. The contrast in pole cancelation behavior between Cu and Mo may lead a reader to suspect that there is some simple way to predict in which systems poles occur in the range of integration. In our experience with these and numerous other systems, we have not been able to do this. Indeed, as a function of $\ell_{\max}$ and iteration number (on the way to charge self-consistency) we find that poles can appear or disappear. What matters is that we know how to determine when we have to deal with them.

Finally, it should be pointed out that the symmetry-adapted functions $T_\ell(\theta,\phi)$ are not used in our computer codes because using them would restrict the generality of the codes. Rather, the charge density is expanded in ordinary spherical harmonics as in Eq. (38), and the group-theoretical relations are used as a check on the accuracy of the calculations.

ACKNOWLEDGMENTS

We thank M. Eisenbach and D. M. Nicholson for their useful discussions. This material is based upon work supported as part of the Center for Defect Physics in Structural Materials, an Energy Frontier Research Center (EFRC) funded by the US Department of Energy, Office of Science, and Office of Basic Energy Sciences.

[1] Lord Rayleigh, Philos. Mag. **34**, 481 (1892).
[2] J. Korringa, Physica **13**, 392 (1947).
[3] W. Kohn and N. Rostoker, Phys. Rev. **94**, 1111 (1954).
[4] P. Hohenberg and W. Kohn, Phys. Rev. B **136**, 864 (1964); W. Kohn and L. J. Sham, **140**, 1133 (1965).
[5] P. H. Dederichs, B. Drittler, and R. Zeller, in *Application of Multiple Scattering Theory to Material Science*, edited by W. H. Butler,

P. H. Dederichs, A. Gonis, and R. L. Weaver, MRS Symposia Proceedings No. 253 (Material Research Society, Pittsburgh, 1992), p. 185.

[6]J. Zabloudil, R. Hammerling, L. Szunyogh, and P. Weinberger, *Electron Scattering in Solid Matter* (Spring-Verlag, Berlin, 2005).

[7]G. M. Stocks, *presented at the KKR Workshop*, Canterbury, England, 2008 (unpublished).

[8]A. Rusanu, presented at the *KKR Workshop*, Budapest, Hungary, 2009 (unpublished).

[9]J. S. Faulkner and G. M. Stocks, Phys. Rev. B **21**, 3222 (1980).

[10]Throughout this paper, when we focus on the nth cell, we take the origin of the system of the coordinate to be at the nucleus of the atom in that cell.

[11]D. D. Johnson, F. J. Pinski, and G. M. Stocks, Phys. Rev. B **30**, 5508 (1984).

[12]G. M. Stocks, W. M. Temmerman, and B. L. Gyorffy, Phys. Rev. Lett. **41**, 339 (1978).

[13]R. Zeller and P. H. Dederichs, Phys. Rev. Lett. **42**, 1713 (1979).

[14]Y. Wang, G. M. Stocks, W. A. Shelton, D. M. C. Nicholson, Z. Szotek, and W. M. Temmerman, Phys. Rev. Lett. **75**, 2867 (1995).

[15]J. S. Faulkner, Phys. Rev. B **19**, 6186 (1979).

[16]A. Gonis and W. H. Butler, *Multiple Scattering in Solids* (Springer-Verlag, New York, 2000).

[17]T. Kotani and H. Akai, Phys. Rev. B **54**, 16502 (1996).

[18]M. Ogura and H. Akai, J. Phys. Condens. Matter **17**, 5741 (2005).

[19]S. L. Altmann and A. P. Cracknell, Rev. Mod. Phys. **37**, 19 (1965).